Segmentation of the lateral ventricles in 3D ultrasound images of the brain in neonates

Bruno Sciolla, Matthieu Martin, Philippe Delachartre, Philippe Quétin

Segmentation of the lateral ventricles in 3D ultrasound images of the brain in neonates

Bruno Sciolla, Matthieu Martin
and Philippe Delachartre
CREATIS laboratory, INSA Lyon, France
Email: bruno.sciolla@creatis.insa-lyon.fr

Philippe Quetin
CH Avignon, France

***Abstract*—The diagnosis and prognosis of brain anomalies in preterm neonates can be improved by the quantification of the cerebral volumes of different brain areas, such as the ventricles [1]. In the current clinical routine, a diagnosis is made based on 2D images of the brain, without making quantitative assessment of the volumes of the cerebrospinal fluid in the ventricles. We propose a semi-automated segmentation method to determine the volume of the ventricles, the choroid plexus, the cavum vergae and the cavum pellucidum in 3D ultrasound images of the brain. The algorithm requires only three seed points given by the operator. We show the good agreement between the segmented contours and manually segmented images on clinical data acquired with a commercial neonatal head probe.**

I. Introduction

The diagnosis and prognosis of prematurely born children can be improved with quantitative measurements of volumes in the brain [1]. In particular, larger ventricles volumes are correlated with neurodevelopmental impairments at 2 years, such as cerebral palsy, hearing loss, blindness or delayed cognitive performance as found in MRI [2], [3], [1]. Larger ventricles are associated with intra-ventricular hemorrhage or primitive ventricular dilatation, both of which are good predictors of cerebral palsy of very preterm infants [4]. The ventricular volumes allow to estimate the ventricular brain ratio [3], which is strongly associated with brain lesions. Indeed, the severity and the evolution of a ventricular dilatation is a good prognosis indicator, in the case of white matter atrophy (hydrocephalus ex-vacuo). Based on this evaluation, a clinician decides whether to plan for surgery or not for posthemorrhagic ventricular dilatation.

In current clinical practice, the ventricular dilatation is evaluated based on measures in cross-sectional cranial ultrasound images. Yet, several procedures have been proposed to quantify the dilatation [5], [6] in cross-sectional images, with no accepted standard. Moreover, there is a large uncertainty about the normal ranges [7], especially for very preterms infants. New longitudinal reference curves have been proposed in recent studies [8], yet it is clear that estimating ventricular dilatation from 2D cross-sectional images is less precise and less clinically relevant than directly estimating the volumes directly in 3D.

It is currently feasible to acquire 3D ultrasound images of the brain with manual sweeping, using standard commercial neonatal head probes. This is rarely done in clinical routine however, because of the lack of operational tools to make quantitative, clinically relevant measurements on 3D images. To estimate the ventricular dilatation, a manual segmentation would be necessary, which is very time-consuming and impractical. To address this issue, we propose a semi-automated method to segment the ventricles, the choroid plexus and the septum pellucidum using only three seed points given by the operator. A convex segmentation algorithm [9] has been previously proposed to segment the ventricles. Compared with this approach, our method requires less input from the user, only 3 points whereas the work [9] requires annotation of several planes to work. Instead, we use geometrical priors on the location of the area of interest and a two-step segmentation process. Notice, however, that we do not claim that our method has the same robustness as in [9].

II. Method

A. Data acquisition

3D images are acquired with a Siemens Acuson 10V4 Transducer through the anterior fontanelle as depicted in Fig. 1. The probe is oriented in the coronal plane and swept manually at angles in a range of 90 degrees. Volumic images are then reconstructed using the Siemens S2000 platform. Because of the manual sweeping, the quality of the volumes is operator dependent, and we keep in this study only volumes with satisfactory quality.

B. Processing chain

The processing chain is shown in Fig. 2a. The images are first registered (rotated) to conform to the standard axial/sagittal/coronal representation used in MRI. This facilitates the reading of 3D ultrasound images for a physician trained to read MRI images. Then a feature map is computed using a phase asymmetry criterion [2], applied to denoised images, which helps in the detection of the boundaries of the ventricles. The user specifies three initialization seeds: one in each lateral ventricle and one in the cavum septum pellucidum, overlapping with the choroid plexus which appear as hyperechogenic regions.

The segmentation is performed in two steps:

1) Segmentation 1: The hypoechogenic regions of the cerebrospinal fluid in the ventricles, in the cavum septum pellucidum and in the cavum vergae are segmented.

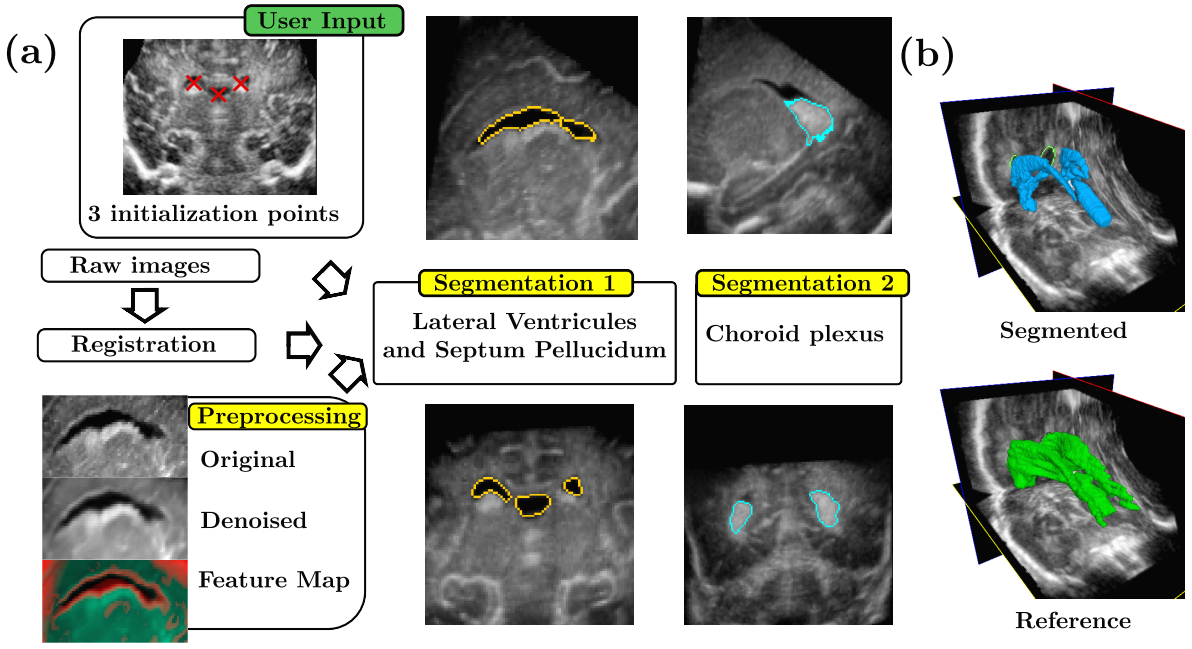

Fig. 2. **(a)** Processing chain including the user initialization, the preprocessing step and the two segmentations. **(b)** Example of a segmented volume, compared with the expert reference.

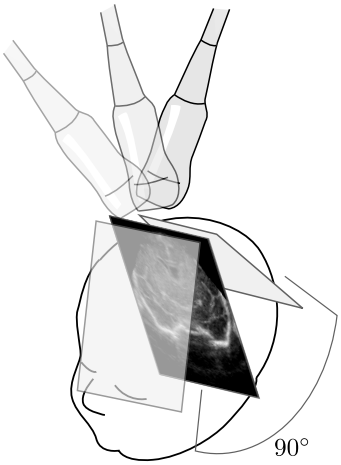

Fig. 1. Anterior fontanelle sonography. Using manual angular sweeping, a 3D image can be reconstructed from a sequence of images.

2) Segmentation 2: The hyperechogenic regions of the choroid plexus are segmented.

The segmentation algorithm is described in the next section.

C. Active contour segmentation

We propose an active contour segmentation where the contour is parametrized implicitly using a level-set function. Specifically, a point in the volume $\mathbf{x}$ belongs to the region of interest A if $\phi_{\mathbf{x}} \geq 0$ and belongs to the background region B for $\phi_{\mathbf{x}} < 0$. The result of the segmentation is the contour which minimizes an objective function $E[\phi]$. The objective function contains a regularization $E^{\text{reg}}[\phi]$, and a data term $E^{\text{data}}[\phi]$.

$$E[\phi] = \alpha E^{\text{reg}}[\phi] + \beta E^{\text{data}}[\phi] + \gamma E^{\text{geom}}[\phi] \quad (1)$$

$$E^{\text{reg}}[\phi] = \int_{\partial A} d\mathbf{x} = \text{Surf}(\partial A) \quad (2)$$

where ∂A is the boundary of region A. The smoothing term $E^{\text{reg}}[\phi]$ is proportional to the area of the boundary. The data term is based on the local intensity $I_{\mathbf{x}}$ and the value of a boundary map $\text{FA}_{\mathbf{x}}$, the Feature Asymmetry (FA), described below. Assuming that $I_{\mathbf{x}}$ and $\text{FA}_{\mathbf{x}}$ are random variables with distributions $P_A^1(I)$, $P_A^2(\text{FA})$ in region A ($P_B^1(I)$, $P_B^2(\text{FA})$ in region B), the data term is proportional to the log of the likelihood of a given contour [10] [11]:

$$E^{\text{data}}[\phi] = -\sum_{\mathbf{x}\in A} \log\left(P_A^1(I_{\mathbf{x}}) P_A^2(\text{FA}_{\mathbf{x}})\right) + (\cdots)_{A\leftrightarrow B} \quad (3)$$

where $(\cdots)_{A\leftrightarrow B}$ is the same term with A exchanged with B. The probability density function $P_A^1(I)$ is estimated using a Parzen estimate, in a non-parametric way [12]:

$$P_A^1(I) = \textstyle\sum_{\mathbf{x}\in A} K_\zeta(I_{\mathbf{x}} - I)/N_A \quad (4)$$

where N_A is the number of voxels in A and K_ζ is Gaussian of standard deviation ζ. The density functions P_A^1 and P_B^1 are updated at each step of the gradient descent used to minimize $E[\phi]$.

The geometric term E^{geom} is used when there is a geometrical prior on the location of the area of interest:

$$E^{\text{geom}}[\phi] = \sum_{\mathbf{x}\in A} g_{\mathbf{x}} \quad (5)$$

Regions with positive cost $g_{\mathbf{x}} > 0$ are penalized and regions with $g_{\mathbf{x}} < 0$ are favored. The geometric term is used in the segmentation 1, and constrains the segmentation to remain in the central cranial region, away from the cranial bones and or shadow areas at the boundaries of the image. In segmentation 2, the geometric term is used to constrain the segmentation to stay close to the ventricles and septum pellucidum found in the first segmentation. This criterion is applied mostly in the frontal region, where the choroid plexus can not have far extensions. In order to implement this constraint of being far from/being away from a region C, we compute a distance map $d_C(\mathbf{x})$ of point $\mathbf{x}$ to the closest point in C. The geometric constraint "being close to C" is obtained with $g_{\mathbf{x}} = |d_C(\mathbf{x}) - d_0|^+$ where d_0 is the allowed distance and $|x|^+ = (|x| + x)/2$ is the positive part. The geometric constraint "being far from C" is $g_{\mathbf{x}} = |d_0 - d_C(\mathbf{x})|^+$.

D. Feature asymmetry (FA) map

The images are first denoised using 3D complex wavelets [13]. Then, as in Ref. [14], the monogenic transform of the volume is computed [15], which allows one to define even/odd quadrature components of the image $I_{\mathbf{x}}$ as:

$$f_e = I * \mathscr{G} \tag{6}$$

$$f_o = \sqrt{(I * \mathscr{G} * h_x)^2 + (I * \mathscr{G} * h_y)^2 + (I * \mathscr{G} * h_z)^2} \tag{7}$$

We use a Log-Gabor filter $\mathscr{G}$, and Riesz functions $h_i(\mathbf{k}) = -j\langle \mathbf{k}, \mathbf{e}_i \rangle / |\mathbf{k}|$ in Fourier space, and $*$ stands for 3D convolution. The feature asymmetry is then computed from the even/odd components following [16]:

$$\mathrm{FA}(\mathbf{x}) = \frac{\sum_p ||f_{e,p}(\mathbf{x})| - |f_{o,p}(\mathbf{x})| - T_M|^+}{\sum_p \sqrt{f_{e,p}(\mathbf{x})^2 + f_{o,p}(\mathbf{x})^2} + \varepsilon} \tag{8}$$

where $\varepsilon = 10^{-4}$, p denotes the 5 different scales of filtering, T_M is a threshold and $|.|^+$ is the positive part. The parameters have been optimized for best accuracy of the contours. Fig. 2 shows the feature map around the ventricle area. The role of the feature map is to increase the accuracy of the ventricle segmentation in narrow regions.

III. Results

We assert the precision of the proposed method on a volume with manually drawn reference, shown in Fig. 2b. In order to quantify the error, we compute the Mean Absolute Distance (MAD) defined as follows. Let us call S the boundary of the segmented volume and N_S the number of voxels in it. We define $d_i^{S \leftrightarrow R}$ the shorter distance between the i-th voxel in the boundary S to any voxel in the reference surface R. Then the MAD is the mean distance $\mathrm{MAD} = \frac{1}{N_S} \sum_{i=1}^{N_S} d_i^{S \leftrightarrow R}$. We find that the MAD of the segmented contour to the reference is of 5.4 pixels, or 2.7 mm.

Fig. 3 shows a different case and three axial slices, compared with the manual reference contour. The in-plane MAD is of $\mathrm{MAD} = 1.24, 1.62, 0.90$ mm on the three slices shown. The agreement between the expert annotations and the segmentation is excellent on this case.

IV. Conclusion

This work is a step towards segmenting more brain regions and make more thorough volume estimations for the neonate brain. In MRI, full brain segmentation has been demonstrated, allowing to use multi-criterion prognosis. The purpose of bringing such tools in ultrasound is to make longitudinal studies with several repeated examinations, which would be costly and not feasible in MRI. Ultrasound is also used in clinical routine, making it possible to put forward systematic 3D ultrasound imaging and volume estimations as a clinical diagnostic and prognosis tool.

Acknowledgment

This work was funded by the ANR-14-LAB3-0006-01 LabCom AtysCrea and was supported by the LABEX CeLyA (ANR-10-LABX-0060) of Université de Lyon, within the "Investissements d'Avenir" program (ANR-11-IDEX-0007) operated by the French National Research Agency (ANR).

References

[1] A. Lind, R. Parkkola, L. Lehtonen, P. Munck, J. Maunu, H. Lapinleimu, L. Haataja, P. S. Group *et al.*, "Associations between regional brain volumes at term-equivalent age and development at 2 years of age in preterm children," *Pediatric radiology*, vol. 41, no. 8, pp. 953–961, 2011.

[2] E. R. Melhem, A. H. Hoon Jr, J. T. Ferrucci Jr, C. B. Quinn, E. M. Reinhardt, S. W. Demetrides, B. M. Freeman, and M. V. Johnston, "Periventricular leukomalacia: Relationship between lateral ventricular volume on brain mr images and severity of cognitive and motor impairment 1," *Radiology*, vol. 214, no. 1, pp. 199–204, 2000.

[3] J. Maunu, R. Parkkola, H. Rikalainen, L. Lehtonen, L. Haataja, H. Lapinleimu *et al.*, "Brain and ventricles in very low birth weight infants at term: a comparison among head circumference, ultrasound, and magnetic resonance imaging," *Pediatrics*, vol. 123, no. 2, pp. 617–626, 2009.

[4] P.-Y. Ancel, F. Livinec, B. Larroque, S. Marret, C. Arnaud, V. Pierrat, M. Dehan, N. Sylvie, B. Escande, A. Burguet *et al.*, "Cerebral palsy among very preterm children in relation to gestational age and neonatal ultrasound abnormalities: the EPIPAGE cohort study," *Pediatrics*, vol. 117, no. 3, pp. 828–835, 2006.

[5] M. I. Levene, "Measurement of the growth of the lateral ventricles in preterm infants with real-time ultrasound." *Archives of Disease in Childhood*, vol. 56, no. 12, pp. 900–904, 1981.

[6] M. Davies, M. Swaminathan, S. Chuang, and F. Betheras, "Reference ranges for the linear dimensions of the intracranial ventricles in preterm neonates," *Archives of Disease in Childhood-Fetal and Neonatal Edition*, vol. 82, no. 3, pp. F218–F223, 2000.

[7] M. J. Brouwer, L. S. De Vries, L. Pistorius, K. J. Rademaker, F. Groenendaal, and M. J. Benders, "Ultrasound measurements of the lateral ventricles in neonates: why, how and when? A systematic review," *Acta Paediatrica*, vol. 99, no. 9, pp. 1298–1306, 2010.

[8] M. J. Brouwer, L. S. de Vries, F. Groenendaal, C. Koopman, L. R. Pistorius, E. J. Mulder, and M. J. Benders, "New reference values for the neonatal cerebral ventricles," *Radiology*, vol. 262, no. 1, pp. 224–233, 2012.

[9] W. Qiu, J. Yuan, J. Kishimoto, J. McLeod, Y. Chen, S. de Ribaupierre, and A. Fenster, "User-guided segmentation of preterm neonate ventricular system from 3D ultrasound images using convex optimization," *Ultrasound in Medicine & Biology*, vol. 41, no. 2, pp. 542 – 556, 2015.

[10] A. Sarti, C. Corsi, E. Mazzini, and C. Lamberti, "Maximum likelihood segmentation of ultrasound images with Rayleigh distribution," *Ultrasonics, Ferroelectrics, and Frequency Control, IEEE Transactions on*, vol. 52, no. 6, pp. 947–960, June 2005.

[11] J. Kim, J. Fisher, A. Yezzi, M. Cetin, and A. Willsky, "A nonparametric statistical method for image segmentation using information theory and curve evolution," *Image Processing, IEEE Transactions on*, vol. 14, no. 10, pp. 1486–1502, Oct 2005.

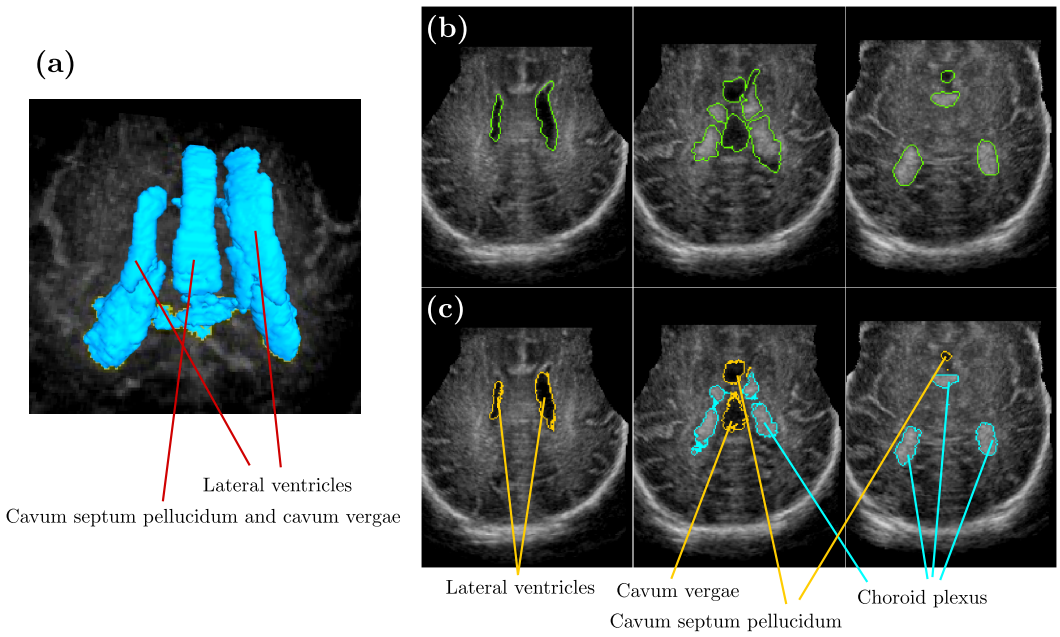

Fig. 3. Segmentation in a case with moderate ventricle dilatation. **(a)** 3D view of the segmented volume, axial view. **(b)** Axial slices with the manual reference for the ventricles, cavum vergae, cavum septum pellucidum and choroid plexus. **(c)** Result of the segmentation. Notice the excellent agreement with the manual reference (b), with a MAD = 1.24, 1.62, 0.90 mm from left to right.

[12] O. Michailovich, Y. Rathi, and A. Tannenbaum, "Image segmentation using active contours driven by the Bhattacharyya gradient flow," *Image Processing, IEEE Transactions on*, vol. 16, no. 11, pp. 2787–2801, Nov 2007.

[13] I. Selesnick, R. Baraniuk, and N. Kingsbury, "The dual-tree complex wavelet transform," *Signal Processing Magazine, IEEE*, vol. 22, no. 6, pp. 123–151, Nov 2005.

[14] K. Rajpoot, V. Grau, and J. Noble, "Local-phase based 3d boundary detection using monogenic signal and its application to real-time 3-d echocardiography images," in *Biomedical Imaging: From Nano to Macro, 2009. ISBI '09. IEEE International Symposium on*, June 2009, pp. 783–786.

[15] M. Felsberg and G. Sommer, "The monogenic signal," *Signal Processing, IEEE Transactions on*, vol. 49, no. 12, pp. 3136–3144, Dec 2001.

[16] P. Kovesi, "Symmetry and asymmetry from local phase," in *Tenth Australian Joint Conference on Artificial Intelligence*, 1997, pp. 2–4.